

ARTICLE

Received 1 Aug 2013 | Accepted 19 Feb 2014 | Published 3 Apr 2014

DOI: 10.1038/ncomms4471

OPEN

Global link between deformation and volcanic eruption quantified by satellite imagery

J. Biggs¹, S.K. Ebmeier¹, W.P. Aspinall¹, Z. Lu², M.E. Pritchard³, R.S.J. Sparks¹ & T.A. Mather⁴

A key challenge for volcanological science and hazard management is that few of the world's volcanoes are effectively monitored. Satellite imagery covers volcanoes globally throughout their eruptive cycles, independent of ground-based monitoring, providing a multidecadal archive suitable for probabilistic analysis linking deformation with eruption. Here we show that, of the 198 volcanoes systematically observed for the past 18 years, 54 deformed, of which 25 also erupted. For assessing eruption potential, this high proportion of deforming volcanoes that also erupted (46%), together with the proportion of non-deforming volcanoes that did not erupt (94%), jointly represent indicators with 'strong' evidential worth. Using a larger catalogue of 540 volcanoes observed for 3 years, we demonstrate how this eruption–deformation relationship is influenced by tectonic, petrological and volcanic factors. Satellite technology is rapidly evolving and routine monitoring of the deformation status of all volcanoes from space is anticipated, meaning probabilistic approaches will increasingly inform hazard decisions and strategic development.

¹School of Earth Sciences, University of Bristol, Queen's Road, Bristol BS8 1RJ, UK. ²Roy M. Huffington Department of Earth Sciences, Southern Methodist University, P.O. Box 750395, Dallas, Texas 75275-0395, USA. ³Department of Earth and Atmospheric Sciences, Cornell University, Ithaca, New York 14853, USA. ⁴Department of Earth Sciences, University of Oxford, South Parks Road, Oxford OX1 3AN, UK. Correspondence and requests for materials should be addressed to J.B. (email: juliet.biggs@bristol.ac.uk).

Volcanic unrest is characterized by changes in seismicity, deformation, gas emissions or fumarolic activity¹. An unrest episode may, or—sometimes crucially—may not lead to eruption². When changes do occur, any lack of baseline information complicates the task of distinguishing between background and precursory activity. Satellite radar (InSAR) can provide high-resolution maps of deformation, allowing the detection of unrest at many volcanoes that may otherwise go unrecognized³. At a well-studied volcano, these data form one part of a multiparameter assessment, but are often the only source of information for remote or inaccessible volcanoes⁴.

Although InSAR is burgeoning as a retrospective scientific tool for understanding magmatic plumbing systems⁵, uptake of such data by volcano observatories has been restricted¹. Critical and timely decisions are often required based on uncertain data and probabilistic tools, such as event trees⁶ and Bayesian Belief Networks⁷, which provide impartial, quantified and defensible information⁸. Only a few frequently erupting and well-monitored volcanoes have a recorded history spanning sufficient periods of unrest and eruption to populate probability tables based on their past behaviour alone.

Rather than relying on this small number of systems, we assess the global statistical relationships using remote observations. Although the multidecadal or shorter timescale of InSAR observations is short compared with many volcano repose periods, by observing a large number of volcanoes at different stages of their eruptive cycle, we adopt an ergodic assumption and substitute geographic coverage for catalogue time length. We then show how tectonic, petrological and volcanic factors influence this relationship.

Results

Global contingency table. For each of the 540 volcanoes that comprise systematic InSAR studies (Fig. 1), we define two distinct underlying traits of each volcano: whether they deformed and whether they erupted, and we then use deformed state as a diagnostic test indicator for the probability of at least one eruption having occurred during the period of InSAR observation (Fig. 2). Further details of the catalogue and definitions are provided in the Methods section. To provide global statistics, we select the 198 volcanoes for which there is a full 18-year observation history. Of these, 25 are classified as *DE* (deformed and erupted; in diagnostic test terms, true positives; Supplementary Table 2); 29 are *D \bar{E}* (deformed but did not erupt; false positives; Supplementary Table 3); 9 are *$\bar{D}E$* (erupted, but did not deform; false negatives; Supplementary Table 4) and 135 are *$\bar{D}\bar{E}$* (did not deform or erupt; true negatives; Supplementary Table 5). Thus, of the 54 volcanoes that deformed, 25 (46%) also erupted during the InSAR observation window, while the proportion of false negatives, $\bar{D}E/\bar{D}$, is very low ($\sim 6\%$). From a hazard perspective, false negatives are especially concerning due to potential high impacts associated with unanticipated eruptions. Given typically long repose periods⁹ and relatively short observation window, it is not surprising that the most common classification is *$\bar{D}\bar{E}$* (68% of volcanoes), but we think this is likely to decrease as observations continue.

From these values, we can quantify the statistical link¹⁰ between deformation and eruption for the available InSAR data. Following terminology from medical diagnostic testing, we describe this association in terms of positive and negative predictive values (hereafter referred to as *PPV* and *NPV*), but note that ‘predictive’ in this context refers to trait associations and does not imply deformation precedes eruption. The *PPV* of the contingency table (the proportion of volcanoes that deformed between 1992 and 2010 that also erupted; DE/D) is 0.46.

The *NPV*, that is, the proportion of ‘non-deformed’ volcanoes that did not erupt in the same period ($\bar{D}\bar{E}/\bar{D}$), is 0.94.

Removing cases of deformation attributed to settling and cooling of recent deposits or removing the $\sim 25\%$ of volcanoes at which measurements are not possible even in systematically studied regions¹¹ from the $\bar{D}E$ category does not push *PPV* or *NPV* outside their 95% confidence intervals.

Volcanological and tectonic influences. The petrological, volcanological and tectonic characteristics of volcanoes vary greatly, and we expect these factors to influence the relationship between deformation and eruption. In the simplest conceptual model routinely applied to geodetic observations, magma supplied to a crustal reservoir from beneath is stored within an elastic medium such that surface deformation rate depends on magma supply rate and storage depth alone¹². In reality, petrological properties, phase changes, rheological variations, fluid flow, local stress fields and other processes occurring within the complex volcanic environment may also influence or drive deformation. Therefore, numerous factors, some observable but others not, may be expected to correspond with observed deformation patterns to a greater or lesser extent. These include crustal thickness and storage depth; magma composition and volatile content; edifice type and repose period; tectonic setting and plate motion; stress and strain rates; rheology and observations of seismicity and gas release.

In order to obtain sufficient sampling across all categories, we use an additional 306 tropical volcanoes that were observed for the 3-year period 2007–2010 and select the corresponding 3-year period from the 198 volcanoes that were used for the global compilation. The *PPV* of the 3-year data set of 504 volcanoes is 0.28 and the *NPV* 0.95. Figure 3 then subdivides this catalogue according to volcano type, plate tectonic setting, magma composition and eruptive history¹³ to compare with the 95% confidence intervals of the *PPV* (0.20–0.36) and *NPV* (0.94–0.97) values.

The proportion of eruptions is higher when there has been a historically recorded eruption (0.45), regardless of whether deformation was observed (Fig. 3). Deformation and eruption are most directly linked (a higher *PPV*) for hotspot regions (0.33), basaltic (0.29) and andesitic compositions (0.34). Low volatile content and high magma supply rates contribute to the elastic storage of low compressibility magma in a shallow chamber for a short period before eruption.

The *PPV* is lowest for rhyolite/dacite compositions (0.17), calderas (0.25) and rift settings (0.13). No phonolite or trachyte composition volcanoes deformed during 2007–2010, but the 18-year record shows a low *PPV* for this category too. Magmatic processes associated with the long-term storage of large magma volumes in the shallow crust may produce surface deformation without ensuing eruption (at least within a multi-decadal timescale)¹⁴. Rift settings and low magma flux are associated with longer magma residence times in the shallow crust, more fractionation and crustal assimilation, formation of more evolved magmas and more calderas but less frequent eruptions^{9,15,16}.

We find low *NPVs* for stratovolcanoes (0.94) and those with basaltic (0.93) and andesitic compositions (0.94) due to a high proportion of *DE* volcanoes. Eruptions involving little or no juvenile material¹⁷, highly compressible gas-rich magmas or rapid ascent from great depth may occur with little or no deformation on the weekly to monthly timescales it is possible to detect with InSAR^{11,14}. Stratovolcanoes are more common on continental crust where the stress field, rigidity contrasts and high parental water contents may contribute to deep storage or compressible magmas, which accommodate pressure changes with little surface deformation^{11,18}. Processes associated with

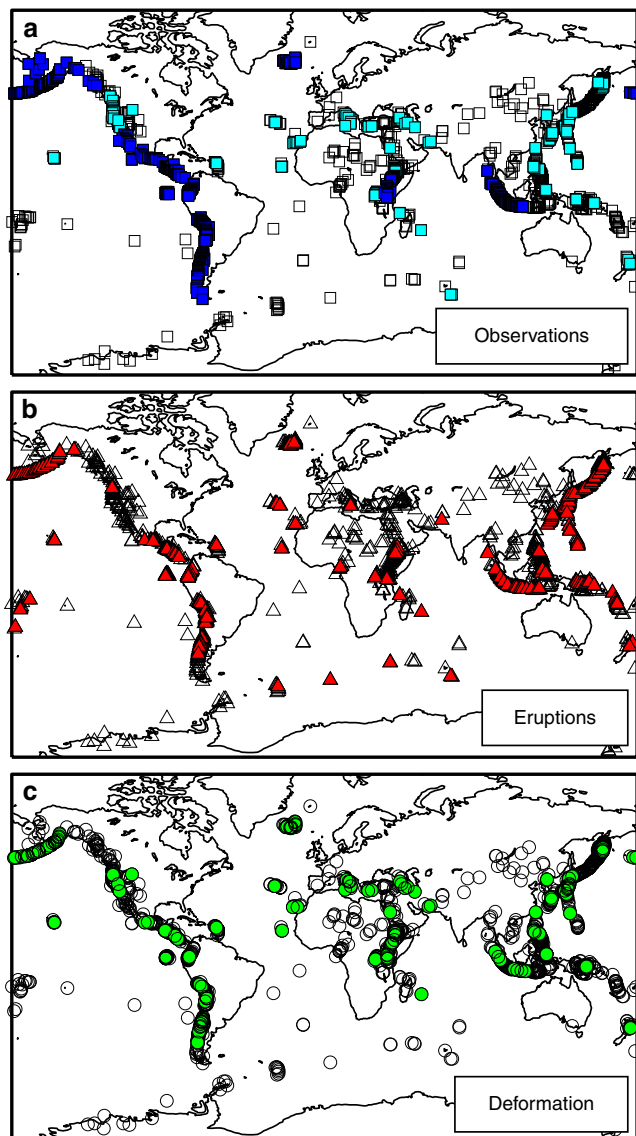


Figure 1 | Global distribution of volcanoes. Locations of 1390 named subaerial Holocene volcanoes from the Global Volcano Database¹³ (all symbols) showing (a) published satellite studies (filled dark blue: systematic studies including null results; filled pale blue: studies of individual volcanoes, 78% of which report eruption or deformation); (b) volcanic eruptions in the Global Volcano Database during the satellite era (filled red), and (c) 165 published reports of deformation, including uplift, subsidence, flow compaction, edifice instabilities and all phases of the eruptive cycle (filled green). See Supplementary Tables 1–5.

conduit pressurization and lava dome extrusion also present challenges for InSAR detection¹⁹.

Relative timing of deformation and eruption. So far, we consider the states ‘deformed’ and ‘erupted’ as two independent, underlying traits, yet defining the temporal and causal links between deformation and eruption is essential for using geodetic observations in a predictive sense. Altering our definitions such that only pre-eruptive deformation is considered a true positive for the 18-year data set (leaving 13 classified as *DE*, and 12 as *DE*) gives a *PPV* value of 0.31 and a *NPV* of 0.92. Both these values are within the 95% confidence intervals of the *PPV* and *NPV* values for the unfiltered data set. Detailed investigation of the timescale of pre-eruptive deformation

based on InSAR observations reveals the strong publication bias towards reporting periods of deformation. Figure 4 covers both individual and systematic studies of *DE* volcanoes and includes all eruptions for which more than 3 years of InSAR data are reported, excluding lava lakes, frequent eruptions (more than one every 3 years) and continuous effusion (Supplementary Table 7). It shows 13 volcanoes that deformed continuously throughout their eruptive cycle and a further 16 where observations began during or after eruption. Deformation is reported to have begun less than a year prior to eruption at Alu in Ethiopia²⁰, El Hierro in the Canaries²¹ and Eyjafjallajökull in Iceland⁵. Interestingly, although Alu and Dalafilla erupted simultaneously, Alu showed pre-eruptive deformation but Dalafilla did not²⁰. Eyjafjallajökull is unique at present in the InSAR record in that it shows multiple short pulses of uplift, two of which did not end in eruption within a year and one that did^{5,22}. Time periods during which no deformation occurred (black bars) are rarely reported explicitly. It is likely that observations continued for over 3 years at several of the volcanoes that were excluded from our analysis but only the time periods during which deformation occurred were reported. Infrequent SAR acquisitions may also obscure the temporal relationship between deformation and eruption, especially where deformation is short-lived.

Discussion

Volcanoes that erupted during the observation window are ~4 times more likely to have recorded deformation than not (the positive likelihood ratio), meaning this information provides ‘strong’ evidential worth²³. However, a *PPV* of 0.46 indicates that deformation alone, while worthy of concern, should not be considered a strong diagnostic of imminent eruption. Moreover, the much greater *NPV* is important because although much emphasis is placed on the ability of volcanologists to predict eruptions, often the ability to make a valid negative deduction can be very valuable for hazard and risk decisions.

Statistical tests on ground-based data (primarily seismicity) indicate that pre-eruptive unrest duration varies between volcano types: from 2 days at complex¹³ volcanoes to 5 months at shield volcanoes²⁴. Radar images of the majority of the world’s volcanoes are only acquired a few times per year, so deformation on these timescales is only resolvable at the handful of volcanoes for which multiple satellite constellations provide frequent revisits or those with permanent ground-based deformation monitoring. Due to the publication bias towards periods of deformation, we are not yet able to quantify the causal or temporal relationships between the extent, rates, timing, amount and duration of deformation and subsequent eruption using InSAR alone. The forthcoming launches of Sentinel-1 and ALOS-2 will greatly increase temporal and spatial resolution and coverage, enabling more subtle distinctions to be incorporated into pattern analysis.

Nonetheless, even with the current data set it is clear that, although the behaviour of individual plumbing systems is often poorly characterized, the statistics for some subsets of global volcanoes (for example, those on rifts, andesite versus rhyolite and so on, Fig. 3) lie outside the global confidence intervals and are consistent with current understanding of tectonic, petrological and volcanological influences. The short eruption cycles at hotspot volcanoes and those of basaltic and andesitic composition mean that the satellite record typically spans both deformation and eruption resulting in a high *PPV*. For volcanoes with long eruption cycles, the satellite record tends to capture either deformation or eruption but rarely both. In the case of rhyolitic, dacitic, phonolitic and trachytic volcanoes and calderas, the inter-eruption period is characterized by shallow magmatic storage producing regular deformation episodes with infrequent

eruptions, resulting in low *PPVs*. In the case of stratovolcanoes, the inter-eruption period is characterized by storage at a range of levels within a thick crust and compressible magmas, producing a high proportion of eruptions without deformation and a relatively low *NPV*. For volcanoes monitored using satellites alone and lacking field measurements, the variation in such diagnostic test statistics associated with globally mapped volcanological and tectonic factors could provide a solid footing for hazard analysis.



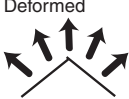

Systematic Coverage	Erupted 	Non-Erupted 
Deformed 	DE 25 True positive	$\bar{D}\bar{E}$ 29 False positive
Non-deformed 	$\bar{D}E$ 9 False negative	$\bar{D}\bar{E}$ 135 True negative

Figure 2 | Contingency table linking volcanoes that deformed and erupted. The table reports the number of occurrences in each category out of the 198 systematically observed volcanoes over 18 years (Table 1, Supplementary Table 1). A volcano that ‘deformed’, *D*, is one where at least one period of deformation has been observed with InSAR, while ‘not deformed’, \bar{D} , means InSAR measurements were made, but that no deformation was reported. ‘Erupted’, *E*, and ‘not erupted’, \bar{E} , volcanoes are those that erupted or not¹³. See Supplementary Tables 2-5 for details of individual volcanoes.

The strength of InSAR lies in its global coverage and remote monitoring capabilities; here we quantify the global link between eruption and deformation on multidecadal hazard assessment timescales. Upcoming technological developments promise to improve the frequency of available images and allow us to quantify the causal or temporal relationships between the extent, rates, timing, magnitude and duration of deformation on shorter timescales. Global studies of volcano deformation have potential to be incorporated into strategic hazard assessments²⁵, particularly in regions with short historical records¹⁵.

Methods

Volcano catalogue. There are 1390 named subaerial Holocene volcanoes¹³ of which 161 have InSAR-based reports of deformation to date and 620 have reported InSAR observations (Fig. 1). Table 1 and Supplementary Table 1 list systematic studies that include discussion of null results: together they cover > 500 volcanoes in the Andes, Central America, Alaska, Africa, Indonesia, Iceland and the Galapagos. The volcanoes in Iceland are not covered by a single systematic study but 85% of them have been included in separate studies of volcanic, seismic, cryospheric or geothermal processes²⁶⁻²⁹ and those in Galapagos are sufficiently close together to be covered by a single satellite frame. InSAR studies outside these regions tend to focus on individual events, such that the proportion of volcanoes that erupted (32%) or deformed (59%) is significantly higher than the corresponding values of 12% and 17% for the systematic studies. Ground-based geodetic networks provide valuable information at higher temporal resolution and over a longer time period than is accessible using InSAR. However, due to the high logistical and financial overheads, they exist only for a small number of volcanoes, often those that are known to be deforming or erupting. Due to the bias away from ‘null results’ associated with individual studies and ground-based networks, we base our subsequent analysis on systematic InSAR studies alone (Table 1).

Due to the high spatial resolution and coverage, InSAR has been very successful in detecting deformation within volcanically active regions. Sometimes, however, this deformation is up to 25 km from any catalogued volcano summit¹³. In these cases, the deformation has been attributed to the closest listed volcano. Supplementary Table 6 lists deformation attributed to a volcano not in the GVP list of Holocene volcanoes.

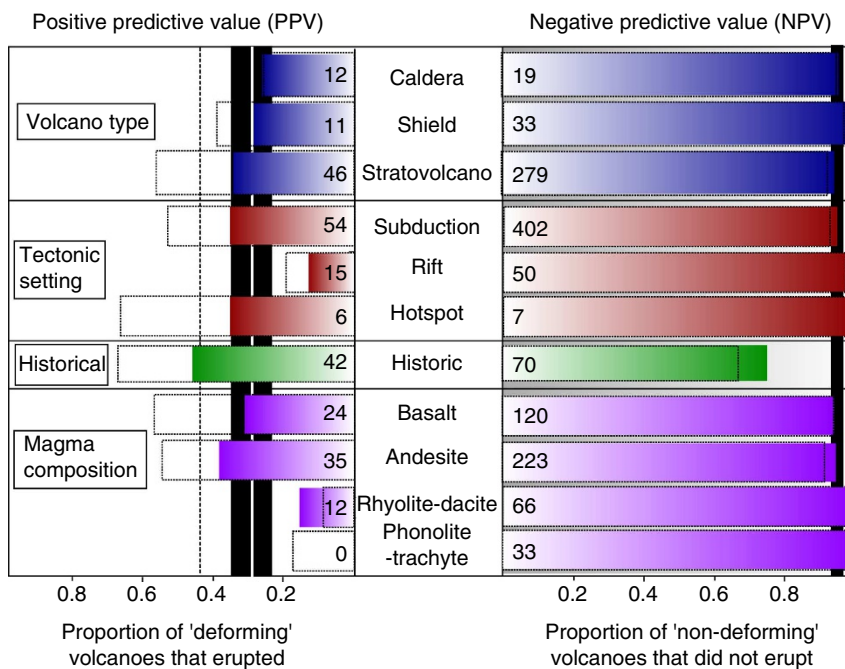


Figure 3 | Subdivision according to volcano characteristics. *PPV* and *NPV* subdivided according to (blue) volcano type¹³ (caldera, shield, stratovolcano); (red) tectonic setting (subduction, rift, hotspot); (green) eruptive history¹³; (purple) magma composition¹³ (basalt, andesite, rhyolite-dacite, trachyte-phonolite). Left side: proportion of volcanoes that deformed that also erupted during the observation period (*PPV*); right side: proportion of volcanoes that did not deform that also did not erupt during the observation period (*NPV*). Coloured bars show values for the 3-year period 2007-2010 for all 540 systematically covered volcanoes and the numbers give the sample size for each category; black outlines show the combined 18-year and 3-year data sets. Black vertical bars mark the 95% confidence bounds on the global values (enclosed white bar) on the 3-year data set, vertical dashed line indicates the global values for the combined data sets.

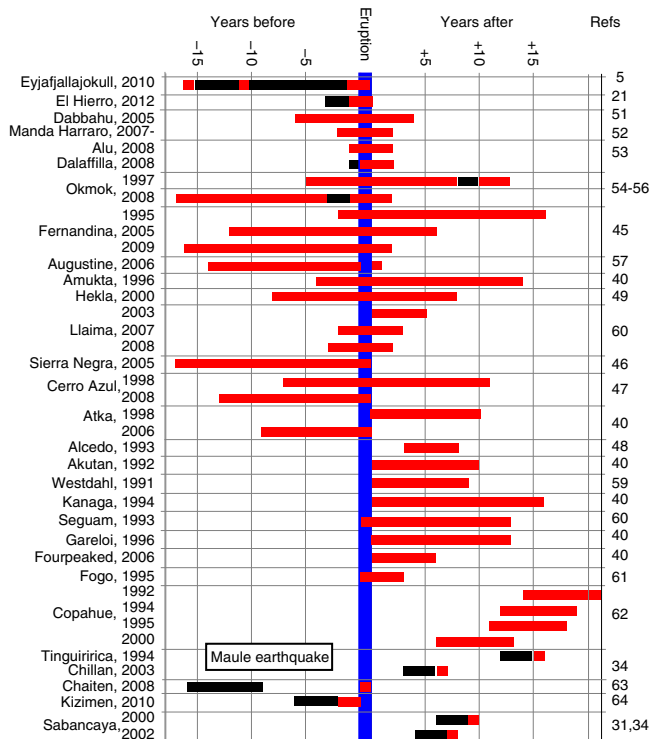


Figure 4 | Relative timing of deformation and eruption for volcanoes. For volcanoes where both deformation (measured by InSAR) and eruption are recorded and more than 3 years of observations are reported (See Supplementary Table 7). Volcanoes with persistent lava lakes, continuous effusion or eruptions more than once per 2-3 years are excluded as continuous ground-based data are more appropriate in these cases. Red bar = deformation; black bar = no deformation; no bar = observation not reported. Volcano name and year of the eruption is given to the left of the figure, references are given to the right of the figure. Note: We use the names from the Global Volcano Database¹³ and refer to the entire region containing ‘Dabbahu’, ‘D’Ure’ and ‘Gabhó’ as ‘Dabbahu’; the region around ‘Ado Ale’ and ‘Wal’is’ as ‘Manda Hararo’, and ‘Korovin’ and ‘Atka’ as ‘Atka’.

Table 1 | List of regional InSAR studies.

Region	Time period	Number	References
East African Rift	1997-2010	38	3,15
Alaska	1992-2010	90	39,40
Central America	2007-2010	117	11,41
Northern Andes	2007-2010	36	32,42
Central Andes	1992-2010	68	31,32,33
Southern Andes	2007-2010	75	31,43
Indonesia	2007-2010	76	33,44
Galapagos	1992-2010	13	45-49
Iceland	1992-2010	27	5,20,22,49-50

These studies report observations at all volcanoes, including those at which no deformation is observed and are compiled to form the catalogue of 540 systematically studied volcanoes used for the statistical analysis of the link between deformation and eruption. Each volcano is assigned two distinct states: either ‘deformed’ or ‘not deformed’ and either ‘erupted’ or ‘not erupted’ which apply to the entire time period regardless of the temporal relationship of deformation and eruption. Further details are given in Supplementary Table 1.

Detection limits. Although InSAR offers an order of magnitude increase in the number of volcanoes that can be observed, several factors limit its ability to detect magmatic processes. The two major limiting factors are as follows: (i) phase delays caused by atmospheric water vapour, particularly the topographically correlated component, and (ii) the loss of signal coherence around snow-capped summits, dense vegetation or steep-sided edifices³⁰. Deep sources may cause small

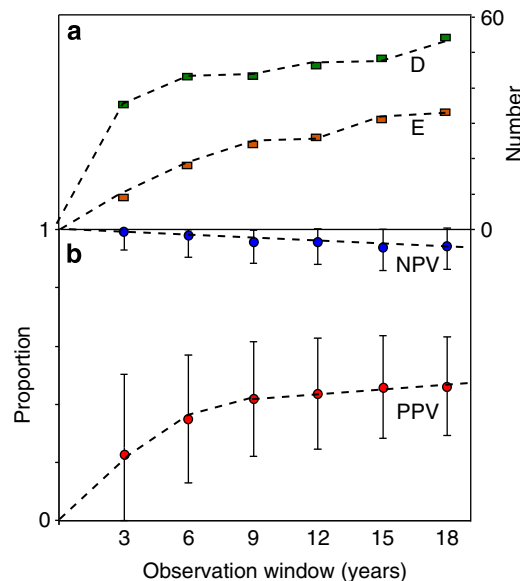


Figure 5 | Effect of observation window length. The effect of observation window length is shown on the number of deforming and erupting volcanoes and the values of *PPV* and *NPV*, calculated using subsets of the 198 volcanoes for which there is an 18-year catalogue. We expect the *PPV* to increase to one over geological timescales, but for the timescales over which decisions are required, it stabilizes at values slightly greater than 0.4 for observation windows > 9 years. (a) Number of volcanoes that erupted (red squares) and number of volcanoes that deformed (green squares). (b) Values of *PPV* (red circles) and *NPV* (blue circles) with 95% confidence intervals.

magnitude deformation signals that fall below the level of atmospheric noise. For shallow processes, such as the emplacement of viscous plugs, the spatial extent of the signal may be restricted to an incoherent area near the vent¹⁹. If the system has an air-magma interface or the magma is compressible¹⁸, volume changes can be accommodated with little or no surface deformation.

Unfortunately, the systematic studies are not uniform in either methodology or error reporting making it difficult to assess how many ‘hidden’ deformation signals exist. Some studies use individual interferograms^{31,32}, others time series methods^{11,33,34}, some report noise thresholds for each volcano¹¹, while others estimate a single value for the survey as a whole^{31,33}, and some do not mention errors at all³⁵. In Central America, time series noise increases by 2 cm for every 1 km of edifice height and measurements are not possible for ~25% of volcanoes covered³⁰. However, there are statistically significant variations in the relationship between the numbers of deformation episodes and historically active volcanoes at volcanic arcs that cannot be attributed to InSAR measurement limitations alone¹¹.

Definitions. Volcanoes show episodic behaviour on timescales ranging between seconds to hundreds of thousands of years⁹ and unrest can take many forms: pulsatory, prolonged, sporadic, reawakening and intra-eruptive²⁴. Deformation can occur in the weeks preceding eruption⁵, many years earlier²² and for months or years afterwards³⁶. Despite this, there is a tendency to conflate the term ‘deformation’ with ‘precursory inflation’, even though many sources of volcano deformation are non-magmatic³⁶ and few are directly followed by an eruption.

Although using the satellite archive allows us to consider a large set of volcanoes, the newness of the technology restricts the timescales observed. The current satellite-based deformation record spans 20 years in some temperate regions but only 3 years in the tropics (Table 1) providing a limited snapshot, especially at volcanoes with long eruption cycles. Conversely, rapid cycles of deformation and eruption may not be captured by satellite repeat intervals of 35-46 days^{19,37,38}. Therefore, our initial analysis above avoids subjective judgements regarding the temporal and causal links between deformation and eruption by combining pre-, co- and post-eruptive deformation into a single category, initially discarding for our current purposes the notion of ‘precursory inflation’.

A volcano that ‘deformed’, *D*, is one where at least one period of deformation has been observed with InSAR, while ‘not deformed’, \bar{D} , means InSAR measurements were made, but that no deformation was reported. We use the satellite observation windows defined in Table 1 and eruption reports from the

Global Volcano Database¹³ to classify each volcano as ‘erupted’, *E*, or ‘not erupted’, *E̅* during the observation period. The resulting four classifications shown in Fig. 2, ‘deformed and erupted’ (*DE*), ‘deformed but not erupted’ (*DE̅*), ‘not deformed but erupted’ (*DE̅*) and ‘not deformed and not erupted’ (*DE̅E̅*) do not imply any causal link, or even a temporal relationship between any specific eruptions and episodes of deformation (Fig. 2). The subset of observations where deformation precedes eruption is also discussed above.

Observation window. To test the influence of the length of the observation window, we subdivide the observations at the 198 temperate zone volcanoes with an 18-year record into shorter observation windows (3, 6, 9, 12, 15 and 18 years since 1992). The number of volcanoes that deformed and erupted rise as observation window length increases, with a particularly rapid increase over the first 3–6 years (Fig. 5). Over geological timescales, we expect the *PPV* to tend to 1; on shorter timescales, over which hazard decisions are made, the *PPV* is slightly greater than 0.4 for observation windows >9 years (Fig. 5).

References

- Sparks, R. S. J., Biggs, J. & Neuberg, J. W. Monitoring volcanoes. *Science* **335**, 1310–1311 (2012).
- Moran, S. C., Newhall, C. & Roman, D. C. Failed magmatic eruptions: late-stage cessation of magma ascent. *B. Volcanol.* **73**, 115–122 (2011).
- Biggs, J., Anthony, E. Y. & Ebinger, C. J. Multiple inflation and deflation events at Kenyan volcanoes, East African Rift. *Geology* **37**, 979–982 (2009).
- Dzurisin, D. A comprehensive approach to monitoring volcano deformation as a window on the eruption cycle. *Rev. Geophys.* **41**, 1001 (2003).
- Sigmundsson, F. *et al.* Intrusion triggering of the 2010 Eyjafjallajökull explosive eruption. *Nature* **468**, 426–430 (2010).
- Newhall, C. & Hoblitt, R. Constructing event trees for volcanic crises. *B. Volcanol.* **64**, 3–20 (2002).
- Aspinall, W. P., Woo, G., Voight, B. & Baxter, P. J. Evidence-based volcanology: application to eruption crises. *J. Volcanol. Geoth. Res.* **128**, 273–285 (2003).
- Sparks, R. S. J., Aspinall, W. P., Crossweller, H. S. & Hincks, T. K. Risk and uncertainty assessment of volcanic hazards. In *Risk and Uncertainty Assessment for Natural Hazards*. (eds Rougier, J., Sparks, S. & Hill, L. J.) 364–398 (Cambridge University Press, 2013).
- Pyle, D. M. Forecasting sizes and repose times of future extreme volcanic events. *Geology* **26**, 367–370 (1998).
- Beguieria, S. Validation and evaluation of predictive models in hazard assessment and risk management. *Nat. Hazards* **37**, 315–329 (2006).
- Ebmeier, S. K., Biggs, J., Mather, T. A. & Amelung, F. On the lack of InSAR observations of magmatic deformation at Central American volcanoes. *J. Geophys. Res. Solid Earth* **118**, 2571–2585 (2013).
- Mogi, K. Relations between the eruptions of various volcanoes and the deformations of the ground surfaces around them. *B. Earthq. Res. Inst. Univ. Tokyo* **36**, 99–134 (1958).
- Siebert, L. & Simkin, T. *Volcanoes of the World: an Illustrated Catalog of Holocene Volcanoes and their Eruptions*. www.volcano.si.edu (2013).
- Moran, S. C., Kwoun, O., Masterlark, T. & Lu, Z. On the absence of InSAR-detected volcano deformation spanning the 1995–1996 and 1999 eruptions of Shishaldin Volcano, Alaska. *J. Volcanol. Geoth. Res.* **150**, 119–131 (2006).
- Biggs, J., Bastow, I. D., Keir, D. & Lewi, E. Pulses of deformation reveal frequently recurring shallow magmatic activity beneath the Main Ethiopian Rift. *Geochem. Geophys. Geosys.* **12**, Q0AB10 (2011).
- Rooney, T. *et al.* Lithospheric modification during crustal extension in the Main Ethiopian Rift. *J. Geophys. Res.* **112**, B10201 (2007).
- Verbeek, R. D. M. *Krakatau*. 546 (Landsdrukkerij/Nationale drukkerij/Nationaal Aardrijkskundig Instituut, 1884).
- Mastin, L. G., Roeloffs, E., Beeler, N. M. & Quick, J. E. Constraints on the size, overpressure, and volatile content of the Mount St. Helens magma system from geodetic and dome-growth measurements during the 2004–2006 + eruption. *US Geol. Surv. Prof. Pap.* **1750**, 461–488 (2008).
- Albino, F., Pinel, V., Massol, H. & Collombet, M. Conditions for detection of ground deformation induced by conduit flow and evolution. *J. Geophys. Res.* **116**, B06201 (2011).
- Pagli, C. *et al.* Crustal deformation associated with the 1996 Gjalp subglacial eruption, Iceland: InSAR studies in affected areas adjacent to the Vatnajökull ice cap. *Earth Planet. Sci. Lett.* **259**, 24–33 (2007).
- González, P. J. *et al.* Magma storage and migration associated with the 2011–2012 El Hierro eruption: implications for crustal magmatic systems at oceanic island volcanoes. *J. Geophys. Res. Solid Earth* **118**, 4361–4377 (2013).
- Pedersen, R. & Sigmundsson, F. Temporal development of the 1999 intrusive episode in the Eyjafjallajökull volcano, Iceland, derived from InSAR images. *B. Volcanol.* **68**, 377–393 (2006).
- Jeffreys, H. *Theory of Probability*. 459 (Oxford University Press, 1961).
- Phillipson, G., Sobrado, R. & Gottsmann, J. Global volcanic unrest in the 21st century: an analysis of the first decade. *J. Volcanol. Geoth. Res.* **264**, 183–196 (2013).
- Aspinall, W. *et al.* *Volcano Hazard and Exposure in Track II Countries and Risk Mitigation Measures—GFDRL Volcano Risk Study*. NGI Report 20100806, 2011).
- Auriac, A. *et al.* Iceland rising: solid Earth response to ice retreat inferred from satellite radar interferometry and viscoelastic modeling. *J. Geophys. Res. Solid Earth* **118**, 1331–1344 (2013).
- Gourmelen, N. *et al.* Ice velocity determined using conventional and multiple-aperture InSAR. *Earth Planet. Sci. Lett.* **307**, 156–160 (2011).
- Pedersen, R., Jónsson, S., Árnadóttir, T., Sigmundsson, F. & Feigl, K. L. Fault slip distribution of two June 2000 M6.5 earthquakes in South Iceland estimated from joint inversion of InSAR and GPS measurements. *Earth Planet. Sci. Lett.* **213**, 487–502 (2003).
- Vadon, H. & Sigmundsson, F. Crustal deformation from 1992 to 1995 at the Mid-Atlantic Ridge, southwest Iceland, mapped by satellite radar interferometry. *Science* **275**, 194–197 (1997).
- Ebmeier, S. K., Biggs, J., Mather, T. A. & Amelung, F. Applicability of InSAR to tropical volcanoes: insights from Central America. *Geol. Soc. London Spec. Publ.* **380**, 15–37 (2013).
- Pritchard, M. E. & Simons, M. An InSAR-based survey of volcanic deformation in the central Andes. *Geochem. Geophys. Geosys.* **5**, Q02002 (2004).
- Fournier, T. J., Pritchard, M. E. & Riddick, S. N. Duration, magnitude, and frequency of subaerial volcano deformation events: new results from Latin America using InSAR and a global synthesis. *Geochem. Geophys. Geosys.* **11**, Q01003 (2010).
- Chaussard, E. & Amelung, F. Precursory inflation of shallow magma reservoirs at west Sunda volcanoes detected by InSAR. *Geophys. Res. Lett.* **39**, L21311 (2012).
- Henderson, S. T. & Pritchard, M. E. Decadal volcanic deformation in the Central Andes Volcanic Zone revealed by InSAR time series. *Geochem. Geophys. Geosys.* **14**, 1358–1374 (2013).
- Amelung, F., Jónsson, S., Zebker, H. & Segall, P. Widespread uplift and ‘trapdoor’ faulting on Galapagos volcanoes observed with radar interferometry. *Nature* **407**, 993–996 (2000).
- Whelley, P. *et al.* Post-depositional fracturing and subsidence of pumice flow deposits: Lascar Volcano, Chile. *B. Volcanol.* **74**, 511–531 (2012).
- Grapenthin, R., Freymueller, J. T. & Serovetnikov, S. S. Surface deformation of Bezymianny Volcano, Kamchatka, recorded by GPS: the eruptions from 2005 to 2010 and long-term, long-wavelength subsidence. *J. Volcanol. Geoth. Res.* **263**, 58–74 (2013).
- Grapenthin, R., Freymueller, J. T. & Kaufman, A. M. Geodetic observations during the 2009 eruption of Redoubt Volcano, Alaska. *J. Volcanol. Geoth. Res.* **259**, 115–132 (2013).
- Lu, Z. *et al.* Diverse deformation patterns of Aleutian volcanoes from satellite interferometric synthetic aperture radar (InSAR). *Geophys. Monogr. Series* **172**, 249–261 (2007).
- Lu, Z. & Dzurisin, D. *InSAR Imaging of Aleutian Volcanoes: Monitoring a Volcanic Arc from Space* (Springer Praxis, 2014).
- Chaussard, E., Amelung, F. & Aoki, Y. Characterization of open and closed volcanic systems in Indonesia and Mexico using InSAR time series. *J. Geophys. Res. Solid Earth* **118**, 3957–3969 (2013).
- Parks, M. M. *et al.* Co-eruptive subsidence at Galeras identified during an InSAR survey of Colombian volcanoes (2006–2009). *J. Volcanol. Geoth. Res.* **202**, 228–240 (2011).
- Pritchard, M. E., Jay, J. A., Aron, F., Henderson, S. T. & Lara, L. E. Subsidence at southern Andes volcanoes induced by the 2010 Maule, Chile earthquake. *Nat. Geosci.* **6**, 632–636 (2013).
- Philibosian, B. & Simons, M. A survey of volcanic deformation on Java using ALOS PALSAR interferometric time series. *Geochem. Geophys. Geosys.* **12**, Q11004 (2011).
- Bagnardi, M. & Amelung, F. Space-geodetic evidence for multiple magma reservoirs and subvolcanic lateral intrusions at Fernandina Volcano, Galápagos Islands. *J. Geophys. Res. Solid Earth* **117**, B10406 (2012).
- Jónsson, S. Stress interaction between magma accumulation and trapdoor faulting on Sierra Negra volcano, Galápagos. *Tectonophysics* **471**, 36–44 (2009).
- Baker, S. & Amelung, F. Measuring deformation associated with magmatic processes at Cerro Azul Volcano, Galapagos Islands, Ecuador with InSAR. *AGU Fall Meet. Abstr.* **1**, 705 (2009).
- Hooper, A., Segall, P. & Zebker, H. Persistent scatterer interferometric synthetic aperture radar for crustal deformation analysis, with application to Volcán Alcedo, Galápagos. *J. Geophys. Res. Solid Earth* **112**, B07407 (2007).
- Ofeigsson, B. G., Hooper, A., Sigmundsson, F., Sturkell, E. & Grapenthin, R. Deep magma storage at Hekla volcano, Iceland, revealed by InSAR time series analysis. *J. Geophys. Res. Solid Earth* **116**, B05401 (2011).

50. Sturkell, E. *et al.* Volcano geodesy and magma dynamics in Iceland. *J. Volcanol. Geoth. Res.* **150**, 14–34 (2006).
51. Field, L., Blundy, J., Brooker, R. A., Wright, T. & Yirgu, G. Magma storage conditions beneath Dabbahu Volcano (Ethiopia) constrained by petrology, seismicity and satellite geodesy. *B. Volcanol.* **74**, 981–1004 (2012).
52. Grandin, R. *et al.* Transient rift opening in response to multiple dike injections in the Manda Hararo rift (Afar, Ethiopia) imaged by time-dependent elastic inversion of interferometric synthetic aperture radar data. *J. Geophys. Res. Solid Earth* **115**, B09403 (2010).
53. Pagli, C. *et al.* Shallow axial magma chamber at the slow-spreading Erta Ale Ridge. *Nat. Geosci.* **5**, 284–288 (2012).
54. Lu, Z., Masterlark, T. & Dzurisin, D. Interferometric synthetic aperture radar study of Okmok volcano, Alaska, 1992–2003: Magma supply dynamics and postemplacement lava flow deformation. *J. Geophys. Res. Solid Earth* **110**, B02403 (2005).
55. Lu, Z., Dzurisin, D., Biggs, J., Wicks, C. & McNutt, S. Ground surface deformation patterns, magma supply, and magma storage at Okmok volcano, Alaska, from InSAR analysis: 1. Interruption deformation, 1997–2008. *J. Geophys. Res. Solid Earth* **115**, B00B02 (2010).
56. Lu, Z. & Dzurisin, D. Ground surface deformation patterns, magma supply, and magma storage at Okmok volcano, Alaska, from InSAR analysis: 2. Coeruptive deflation, July–August 2008. *J. Geophys. Res.* **115**, B00B03 (2010).
57. Lee, C. W., Lu, Z., Kwoun, O. I. & Won, J. S. Deformation of the Augustine Volcano, Alaska, 1992–2005, measured by ERS and ENVISAT SAR interferometry. *Earth Planets Space* **60**, 447–452 (2008).
58. Bathke, H., Shirzaei, M. & Walter, T. R. Inflation and deflation at the steep-sided Llaima stratovolcano (Chile) detected by using InSAR. *Geophys. Res. Lett.* **38**, L10304 (2011).
59. Lu, Z., Masterlark, T., Dzurisin, D., Rykhus, R. & Wicks, C. Magma supply dynamics at Westdahl volcano, Alaska, modeled from satellite radar interferometry. *J. Geophys. Res. Solid Earth* **108**, 1567–1570 (2003).
60. Lee, C. W., Lu, Z., Won, J. S., Jung, H. S. & Dzurisin, D. Dynamic deformation of Seguam Island, Alaska, 1992–2008, from multi-interferogram InSAR processing. *J. Volcanol. Geoth. Res.* **260**, 43–51 (2013).
61. Amelung, F. & Day, S. InSAR observations of the 1995 Fogo, Cape Verde, eruption: implications for the effects of collapse events upon island volcanoes. *Geophys. Res. Lett.* **29**, 47–51 (2002).
62. Velez, M. L., Euillades, P., Caselli, A., Blanco, M. & Díaz, J. M. Deformation of Copahue volcano: inversion of InSAR data using a genetic algorithm. *J. Volcanol. Geoth. Res.* **202**, 117–126 (2011).
63. Wicks, C., de La Llera, J. C., Lara, L. E. & Lowenstern, J. The role of dyking and fault control in the rapid onset of eruption at Chaitén volcano, Chile. *Nature* **478**, 374–377 (2011).
64. Ji, L., Lu, Z., Dzurisin, D. & Senyukov, S. Pre-eruption deformation caused by dike intrusion beneath Kizimen volcano, Kamchatka, Russia, observed by InSAR. *J. Volcanol. Geoth. Res.* **256**, 87–95 (2013).

Acknowledgements

J.B., S.K.E. and T.A.M. are supported by UK Natural Environment Research Council through the COMET and STREVA programmes. R.S.J.S. and W.P.A. were supported by an ERC Grant to R.S.J.S. (VOLDIES). W.P.A. and R.S.J.S. are also supported by STREVA. M.E.P. was supported by NASA's Science Mission Directorate grant #NNX12AM24G. We thank Carolina Pagli and Jon Blundy for useful discussions.

Author contributions

J.B. and S.K.E. carried out the analysis and J.B. wrote the paper with input from all authors. S.K.E., J.B. and T.A.M. conceived the systematic global approach. W.P.A. contributed to the statistical analysis; J.B., S.K.E., Z.L., M.E.P. contributed to the InSAR data set; J.B., R.S.J.S., S.K.E. and T.A.M. contributed to the interpretation.

Additional information

Supplementary Information accompanies this paper at <http://www.nature.com/naturecommunications>

Competing financial interests: The authors declare no competing financial interests.

Reprints and permission information is available online at <http://www.npg.nature.com/reprintsandpermissions/>

How to cite this article: Biggs, J. *et al.* Global link between deformation and volcanic eruption quantified by satellite imagery. *Nat. Commun.* **5**:3471 doi: 10.1038/ncomms4471 (2014).



This work is licensed under a Creative Commons Attribution 4.0 International License. The images or other third party material in this article are included in the article's Creative Commons license, unless indicated otherwise in the credit line; if the material is not included under the Creative Commons license, users will need to obtain permission from the license holder to reproduce the material. To view a copy of this license, visit <http://creativecommons.org/licenses/by/4.0/>